GEOPHYSICS, VOL. 46, No. 8 (AUGUST 1981); P. 1148–1162, 18 FIGS., 7 TABLES.

GL04069

Three-dimensional resistivity inversion using alpha centers

Wm. R. Petrick, Jr.*, Wm. R. Sill*, and S. H. Ward‡

ABSTRACT

The method of alpha centers represents a class of solutions to the three-dimensional (3-D) dc conduction equation based on certain nonlinear substitutions for electric potential and earth conductivity. A solution is obtained which is sufficiently fast to make the inversion of 3-D resistivity data practical. The inversion routine results in a conductivity distribution defined by α centers which simultaneously fits the data from several parallel or perpendicular dipole-dipole profiles.

To illustrate the characteristics of this modeling approach, we apply the inversion algorithm to three theoretical and four field data sets. The four field data sets represent samples from massive sulfide and geothermal environments. The technique, when applied to theoretical data from prismatic bodies, gives fairly good estimates of the positions of conductive inhomogeneities but poor estimates of their actual conductivities.

The entire inversion algorithm requires less than 15,000 words of computer memory, thus making it tractable for small computers. We envision two major applications. The first is for in-field data interpretation to site drilling locations or to guide further exploration. The second is for obtaining a good initial guess for more sophisticated and costly multidimensional inversion schemes.

INTRODUCTION

Solutions of the dc conduction equation using alpha (α) centers were completely derived by Stefanescu and Stefanescu (1974). In that paper references to the α center method are given which date back to 1950. More recently, α media (the term "alpha media" refers to the conductivity distribution defined by α centers) have been used to calculate magnetometric resistivity responses (Edwards et al, 1978). The method uses nonlinear substitutions for media conductivity and electric potential, followed by a straightforward application of image theory. This results in an economical solution which is exact for α media.

Due to the speed and ease of parameterization of this forward algorithm, it seemed only natural to implement it in an inverse routine. The ridge regression inversion algorithm was chosen because experience with the method has proven it to be stable and simple to implement in a wide variety of inverse applications (Inman, 1975; Rijo et al, 1977; Petrick et al, 1977; Pelton et al, 1978).

We do not maintain that this modeling scheme is ideal, but it seems to be successful in locating the positions of conductive inhomogeneities in the presence of substantial geologic noise. It is also flexible enough to handle multibody problems and problems of mixed dimension. Run times for the examples presented here range from 18 sec to 5.5 minutes on the University of Utah Univac 1108.

THE ALPHA CENTER FORWARD SOLUTION

This development follows Stefanescu and Stefanescu (1974). We start with the general dc conduction equation in inhomogeneous isotropic media

$$\nabla\sigma \cdot \nabla\phi + \sigma\nabla^2\phi = 0, \tag{1}$$

where σ = media conductivity, and ϕ = electric potential. Through use of the transformations $\phi = \psi/\alpha$ and $\sigma = \alpha^2$, equation (1) becomes

$$\alpha\nabla^2\psi - \psi\nabla^2\alpha = 0. \tag{2}$$

Upon separating variables in equation (2), we obtain

$$\frac{\nabla^2\psi}{\psi} = \frac{\nabla^2\alpha}{\alpha} = f(m), \tag{3}$$

where m is any point in a whole space. At this point $f(m)$ is arbitrary and can be chosen so that closed form solutions to equation (3) are obtained. In choosing $f(m)$, we determine the functional form of α which in turn fixes the form of the conductivity distribution since $\sigma = \alpha^2$.

One possible choice for $f(m)$ is $f(m) = k^2$ where k is a real positive constant. This choice of $f(m)$ was the subject of Stefanescu and Stefanescu (1974). It leads to a formulation having α media described by

$$\alpha(m) = \sum_i C_i \frac{e^{-kR_{im}}}{R_{im}} + C_{ii}\frac{e^{+kR_{im}}}{R_{im}},$$

where R_{im} is the distance from point m to the position of the ith α center. We first tested an inversion routine utilizing α media of this type. In all test cases on data generated with prismatic bodies, k was forced to zero resulting in α being a sum of C_i/R_{im} terms.

Another choice for $f(m)$ which results in equation (3) having a closed form solution is $f(m) = 0$. This results in

$$\nabla^2\psi = 0, \nabla^2\alpha = 0. \tag{4}$$

Manuscript received by the Editor October 8, 1979; revised manuscript received August 21, 1980.
*Department of Geology and Geophysics, 717 Mining Science Building, University of Utah, Salt Lake City, UT 84112.
‡University of Utah Research Institute, Earth Science Lab, 420 Chipeta Way, Suite 120, Salt Lake City, UT 84108.

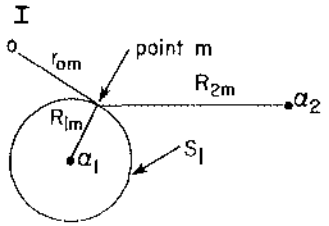

FIG. 1. Relationships between components summarized by equations (7) for two α centers (α_1 and α_2) in a whole-space.

Choosing solutions to $\nabla^2\alpha = 0$ of the form

$$\alpha(m) = B + \sum_i C_i/R_{im} \tag{5}$$

allows us easily to specify a background conductivity (B^2). Because of this ease and the fact that the inversion routine set k to 0, we chose the $f(m) = 0$ solution over the $f(m) = k^2$ solution for the final forward problem.

The solution to $\nabla^2\psi = 0$ which decays with increasing R is

$$\psi(m) = \psi_0 + \sum_i D_i/R_{im}. \tag{6}$$

ψ_0 may be determined by noting that near a current electrode in a whole space the primary electric potential ϕ_0 must behave as $I/4\pi r_{0m}\sigma_0$. Substituting this in $\psi = \phi\alpha$, we have

$$\psi_0 = I/4\pi r_{0m}\alpha_0,$$

where α_0 is the value of α at the current electrode and r_{0m} is the distance from point m to the current electrode.

At this point we have the following relationships:

$$\phi = \psi/\alpha,$$
$$\sigma = \alpha^2,$$

$$\alpha(m) = B + \sum_i C_i/R_{im},$$

$$\psi(m) = I/4\pi r_{0m}\alpha_0 + \sum_i D_i/R_{im}, \tag{7}$$

where B, C_i are chosen positive constants, α_0 = value of α at the current electrode, r_{0m} = distance from current electrode to the point m at which the potential is measured, R_{im} = distance from ith alpha center to the point at which the potential is measured, and D_i = constants to be determined.

The earth conductivity is determined by choosing B, C_i, and the positions of the α centers. Once we determine ψ, we may obtain the electric potential.

The continuity equation

$$\nabla \cdot \bar{\mathbf{J}} + \frac{\partial \rho}{\partial t} = 0,$$

reduces to $\nabla \cdot \bar{\mathbf{J}} = 0$ in the dc case. To determine ψ, we enforce

$$\int \nabla \cdot \bar{\mathbf{J}} dv = 0$$

at each α center. This leads to a set of linear equations to be solved for the coefficients D_i. From the constitutive relation $\mathbf{J} = \sigma\mathbf{E}$ (assuming isotropic media), $\mathbf{E} = -\nabla\phi$, and the relationship given by equation (7), the expression for current density, is

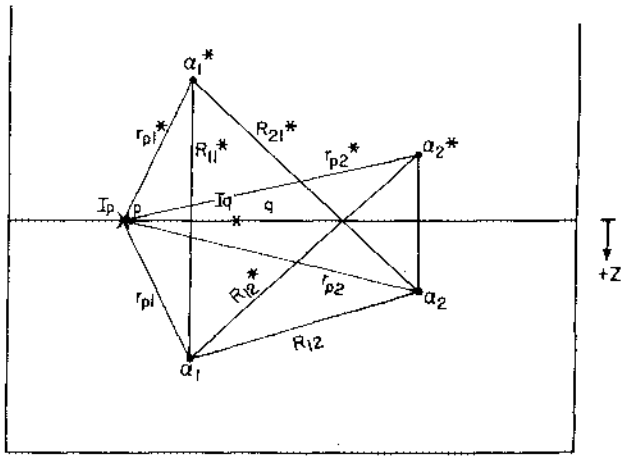

FIG. 2. Relationships between components of α center solution now taking into account current input at point p, current extraction at point q, and image α distribution resulting in a half-space solution. Image components are denoted by asterisks.

$$\bar{\mathbf{J}} = \psi\nabla\alpha - \alpha\nabla\psi. \tag{8}$$

Figure 1 shows the relationships between the components summarized in equations (7) for two alpha centers.

Substituting equation (7) into equation (8) and evaluating the expression at point m, we have

$$J(m) = \left(I/4\pi r_{0m}\alpha_0 + \sum_i D_i/R_{im}\right)\left(-\sum_i C_i \frac{\nabla R_{im}}{R_{im}^2}\right) - \left(B + \sum_i C_i/R_{im}\right)\left[(-I/4\pi\alpha_0)(\nabla r_{0m}/r_{0m}^2) - \sum_i D_i \frac{\nabla R_{im}}{R_{im}^2}\right]. \tag{9}$$

After constructing a sphere of radius R_{jm} about the jth α center, we have

$$\int_{V_j} \nabla \cdot \bar{\mathbf{J}} dv = \int_{S_j} \bar{\mathbf{J}} \cdot \hat{\mathbf{n}} ds_j = \int_{\Omega_j} (\bar{\mathbf{J}} \cdot \nabla R) R_{jm}^2 \, d\Omega = 0,$$

where Ω is the solid angle. Now taking

$$\lim_{R_{jm} \to 0} [\bar{\mathbf{J}}_{\text{radial},\, m} R_{jm}^2] = 0$$

we obtain, noting that as $R_{im} \to 0$ then $R_{jm} \to R_{ij}$,

$$-\left[I/4\pi\alpha_0 r_{0j} + \sum_{\substack{i \\ i \neq j}} D_i \frac{1}{R_{ij}} + D_j/R_{jj}\right] C_j + \left[B + \sum_{\substack{i \\ i \neq j}} C_i/R_{ij} + C_j/R_{jj}\right] D_j = 0.$$

Solving for D, we obtain

$$D_j\left[B + \sum_{\substack{i \\ i \neq j}} C_i/R_{ij}\right] - C_j \sum_{\substack{i \\ i \neq j}} D_i/R_{ij} = C_j I/4\pi\alpha_0 r_{0j}. \tag{10}$$

Equation (10) is valid for a point current source in a whole space. To account for a conductivity distribution in a half-space ($z > 0$) and two current electrodes, consider image α centers as shown in Figure 2. The image components are indicated by

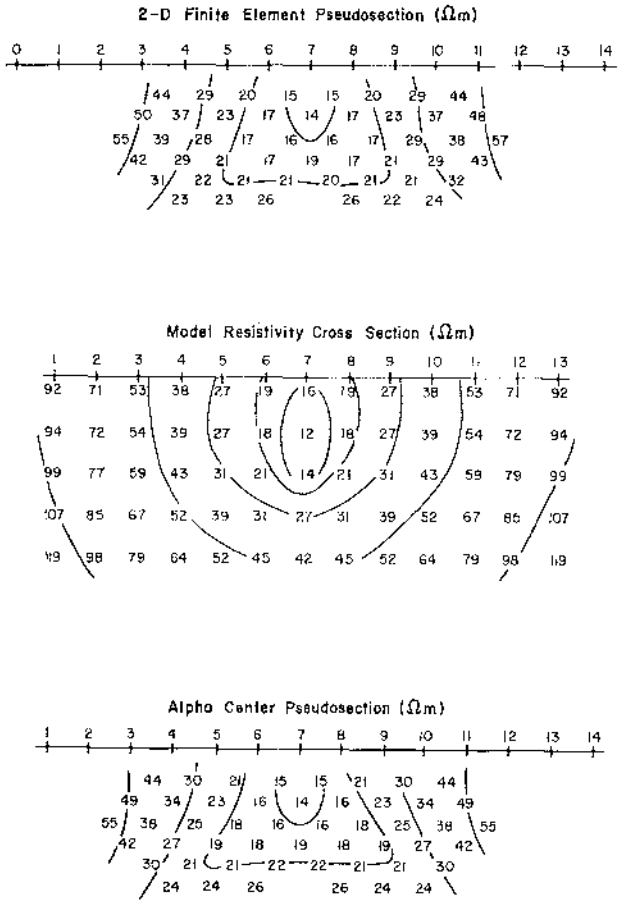

FIG. 3. Comparison of 2-D finite-element solution and α center solution for dipole-dipole array. Electrode spacing is a. The 2-D inhomogeneity is approximated by a string of 36 α centers placed normal to the plane of the section spaced a distance $a/3$ apart at a depth of 1.5 a below electrode seven.

asterisks. Carrying out the same analysis as that leading from equation (9) to equation (10) except now considering current input at point p, extraction at point q, and the image centers, we have

$$D_j\left[B + \sum_{\substack{i \\ i\neq j}} C_i\left(\frac{1}{R_{ij}} + \frac{1}{R^*_{ij}}\right)\right] - C_j\left[\sum_{\substack{i \\ i\neq j}} D_i\left(\frac{1}{R_{ij}} + \frac{1}{R^*_{ij}}\right)\right] = C_j\frac{I}{2\pi}\left[\frac{1}{\alpha_p r_{pj}} - \frac{1}{\alpha_q r_{qj}}\right]. \quad (11)$$

The system of equations defined by equation (11) can now be solved for D. Two important characteristics of this system are (1) the coefficients defining the matrix are source independent, therefore the matrix only need be inverted once for a particular alpha center distribution, and (2) the matrix is guaranteed to be nonsingular for positive coefficients B and C_i.

The function ψ at point m on the plane $z = 0$ due to current injection and extraction on the same plane at points p and q is

$$\psi(m)_{pq} - (I/2\pi)[1/\alpha_p r_{pm} - 1/\alpha_q r_{qm}] + 2\sum_i D_i/R_{im}. \quad (12)$$

The expression for α at point m, where m may now be anywhere in the half-space $z > 0$ (z positive in the earth) is

$$\alpha(m) = B + \sum_i C_i\left(\frac{1}{R_{im}} + \frac{1}{R^*_{im}}\right). \quad (13)$$

The associated electric potential at point m on $z = 0$ is then

$$\phi(m)_{pq} = \psi(m)_{pq}/\alpha(m). \quad (14)$$

From equation (14), the apparent resistivity for any electrode array on the plane $z = 0$ can be calculated. Figure 3 shows a comparison of the apparent resistivities calculated using the α center forward solution and a 2-D finite-element program (Rijo, 1977) for the dipole-dipole array. The agreement is everywhere better than 10 percent. Alpha centers were placed every dipole length/3 normal to the plane of the profile in order to represent a 2-D body. The center of the string of 36 α centers is 1.5 dipole lengths below electrode 7 and has coefficients $B = .001$, $C = 2$. This particular α center body appears 2-D when its strike extent is 11 to 12 dipole lengths. Although 2-D α media responses were presented by Stefanescu and Radulescu (1965), we do not employ that solution due to the programming difficulty that would be encountered when we invert to three dimensional (3-D) bodies in the presence of 2-D bodies.

Figure 4 is an example of the type of conductivity distribution that can be expected with α center modeling. This conductivity distribution is due to two centers located at $r_1 = 500$ m and $r_2 = 600$ m. The three different curves indicate how the conductivity changes by varying the coefficients of the centers with the background conductivity given by B^2 on Figure 4. The conductivity has the form $\sigma = B^2 + 2BC/R + C^2/R^2$ showing a rapid $1/R^2$ fall-off near the α center at $R = 0$ with a slower $1/R$ behavior at greater distance. The smaller the C coefficient, the more rapid the conductivity decrease. Note that with this form for α, it is not possible to consider compact resistive bodies. At $R = 0$ the conductivity becomes infinite so each α center may be thought of as a current sink. By enforcing

$$\int \nabla \cdot \bar{\mathbf{J}} dv = 0$$

at each α center and solving for the associated D_j coefficients, we are determining the strength of artificial current sources which must be applied at each α center. This forces a divergenceless current density everywhere except at true sources.

For an analysis which compares the whole-space uniform electric field response of an α center to that of an infinitely conductive sphere, see the Appendix. Suffice it to say that an α center response is not dipolar. We assert that this lack of a dipolar response is the factor limiting the accuracy with which α center inversion is capable of fitting theoretical data from prismatic bodies.

THE INVERSION ALGORITHM

We have found in practice that by locking together several centers, we can represent responses due to conductive layers, dikes, podiform masses, cylinders or any combination of these fairly successfully. Alpha centers are locked together by fixing intercenter distances while allowing the group to move as a whole. Not only is the forward solution exceptionally fast, but parameterization in α center inversion is conveniently accomplished. The inversion results are not discrete blocks or sharp contacts, but a continuous resistivity distribution which, in some cases, may more nearly reflect the true geologic situation. The method is, however, not without its shortcomings, and we have attempted to illustrate these as well as its advantages in several examples to be presented later.

The actual inversion technique employed is weighted nonlinear

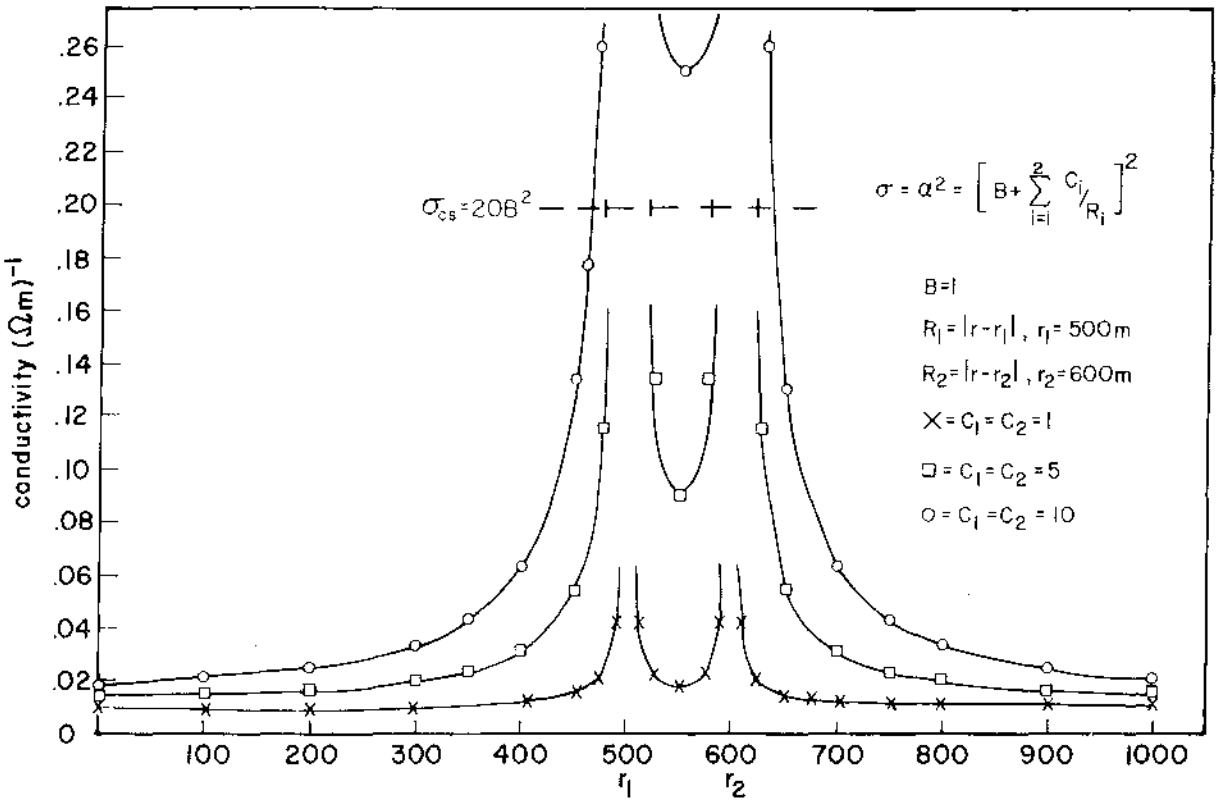

FIG. 4. Conductivity distribution due to two α centers. The three different curves show how the conductivity changes as the coefficients C_i of the α centers are changed. σ_{cs} is the level at which the conductivity is 20 times the background conductivity defined by B^2. r is the distance in meters.

least-squares with ridge regression. Its application to electrical methods has been described in many papers (Inman, 1975; Rijo et al, 1977; Petrick et al, 1977; Pelton et al, 1978), so, to be concise, we refer the reader to these.

After having found a model which best fits the observed data, it is useful to have some idea concerning how well each of our model parameters is determined. We may obtain some feeling for this by examining the parameter covariance matrix, which for weighted least-squares is given by

$$\text{cov}(p) = \chi_\nu^2 (\mathbf{A}^T \mathbf{W}^T \mathbf{W} \mathbf{A})^{-1}, \tag{15}$$

where p is an inversion parameter (in this case, B, C_i, and R_{im}), χ_ν^2 is the reduced chi-square value defined as the weighted least-square error divided by ν (the problem degrees of freedom), $\mathbf{A}$ is a matrix of derivatives, and $\mathbf{W}$ is a data weight matrix.

Taking the square root of the diagonal elements of cov (p) gives us an estimate of the parameter standard deviation, while normalizing equation (15) as follows

$$\text{cor}(p_{ij}) = \frac{\text{cov}(p_{ij})}{[\text{cov}(p_{ii}) \cdot \text{cov}(p_{jj})]^{1/2}} \tag{16}$$

results in parameter correlation coefficients. If the correlation coefficient is near $+1.0$, only the product of two parameters is determined. If it is near -1.0, only the quotient is determined.

To construct the $\mathbf{A}$ matrix, it is necessary to take derivatives of apparent resistivity with respect to parameters of the conductivity distribution, essentially α in this case. Repeating equation (13)

$$\alpha(m) = \sqrt{\sigma(m)} = B + \sum_i C_i \left[\frac{1}{R_{im}} + \frac{1}{R_{im}^*} \right],$$

we see that the conductivity distribution depends upon B, C_i, and the x-, y-, z- coordinates of the α centers. Since B, C_i, and z_i can never be negative, we can most simply ensure this by inverting with respect to log B, log C_i, and log z_i. Derivatives with respect to x_i and y_i are taken with respect to the normal Euclidean space parameters. When several α centers are locked together, the derivative is taken with respect to the component of α in which movement of the entire group is desired. The derivatives are approximated using the first forward difference.

We fit log apparent resistivity data, so the reduced chi-square data variance estimate refers to a percent data error. Similarly, the parameter standard deviation estimates are in terms of percent standard deviation for B, C_i, and z_i while the estimates are in units of meters for the x-, y- coordinates. By percent standard deviation we refer to a measure that is normally distributed about the parameter estimate in log space. For example, if we determine the parameter B to within ± 60 percent, the upper value in Euclidean space is given by $B \times 1.6$ while the lower value is $B/1.6$.

Orginally a program was used which calculated the percent standard deviations of the inverted earth model resistivities from the α center statistics. Experience has shown that the direct α center statistics provide more useful information concerning possible reparameterizations. The reason for this is that the direct α parameter statistics provide an analysis of exactly which aspects of the

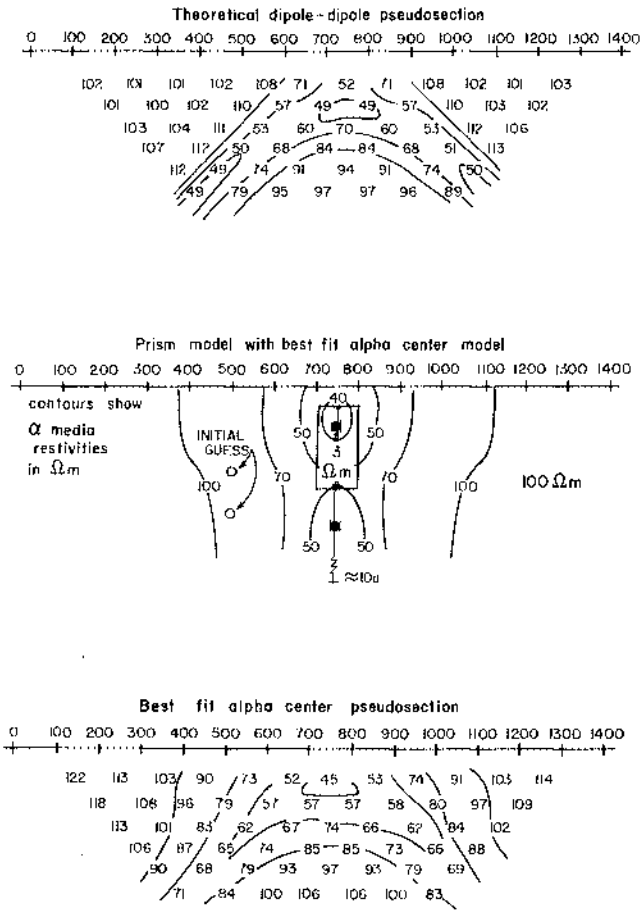

FIG. 5. Test case 1: model 9-3D. Parameterization 3 inversion results using α centers to fit data from a prismatic model. The prismatic body which is bisected by the profile is two dipole lengths in strike and depth extent, has a thickness of one dipole length, and is .5 dipole lengths to the top. The prism has a resistivity of 3Ω-m and is set in a 100 Ω-m background.

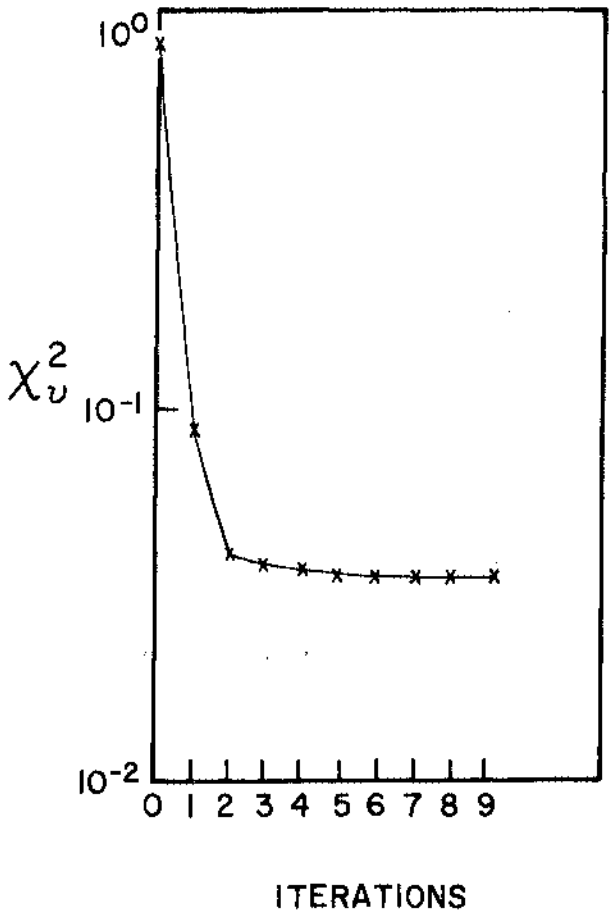

FIG. 6. Convergence for model 9-3D, parameterization three. Reduced chi-square value versus number of iterations.

Table 1. Different parameterizations used to invert prismatic model 9-3D data. $\sigma = \alpha^2 = (B + \Sigma C_i/R_i)^2$. Note that data fit is virtually the same for all parameterizations. *x* denotes an inversion parameter.

Parameterization	B	$C_i = C$	Position Along Profile	Depth To Top α Center	Depth To Lower α Center	Dip	Data Fit
1	x	x	x				20%
2	x	x	x	x			21%
3	x	x	x	x	x		21%
4	x	x	x	x	x	x	21%

Table 2. Alpha center parameters, parameter statistics, and correlation coefficients for model 9-3D, parameterization three.

Parameters	Inverted Model	Parameter Statistics	Correlation Coefficients				
B	$.071\ \sqrt{S/m}$	±25%	1.0				
$C_i=C$	$1.6\ \sqrt{Sm}$	±104%	-.99	1.0			
$x_i=x$	748m	±.14m	.04	-.02	1.0		
z_{Lower}	334m	+225%	-.96	.99	-.01	1.0	
z_{Upper}	91m	±63%	-.95	.95	.04	.93	1.0

model are poorly determined, while resistivity confidence limits represent a combination of all direct α parameter statistics. The one standard deviation error bars on the following plots refer to the direct α parameters B, C_i, x_i, y_i, and z_i.

INVERSE TEST CASES

During the normal course of program development we, of course, assured ourselves that the algorithm was capable of inverting to the correct α conductivity distributions for data generated by α media. A more important practical question concerns the ability of the α inversion to determine the location and conductivities of more general conductive inhomogeneities. To test this ability, we used theoretical data from 3-D conductive prisms. Two data sets were obtained from finite-difference calculations (Dey and Morrison, 1979). The models chosen were a 3-D conductive prism in a half-space (model 9-3D) and Dey and Morrison's Basin and Range geothermal model. A third data set was obtained from G. Hohmann (personal communication) and represents an integral-equation solution of two finite-length vertical dikes in a half-space.

Test case 1: Model 9-3D

The theoretical data shown in Figure 5 are from a profile bisecting the prism perpendicular to its strike. The strike extent is two units.

These data were inverted several times with the different parameterizations shown in Table 1. Since theoretical data were available for only one profile, we constrained the lateral positions of four α centers at ±.5 units with respect to the profile. The rather poor initial guesses for the positions of these centers are indicated by the open circles in the model shown in Figure 5. The α centers are actually constrained to lie at ±.5 units off the profile to mimic the strike extent of the prism.

Table 1 shows that all parameterizations were capable of fitting the theoretical data to within about 20 percent. This is probably about as good a fit to data from prismatic models as we can expect from an α center approximation. Note that the parameterization for inverse four in Table 1 includes dip as an inversion parameter. In this modeling approach, dip is approximated by allowing the lower two α centers to move along the profile independently from the top two centers. We found that the positions along the profile, as well as the depth of these deeper α centers, were very poorly determined parameters supporting the observation that dip is not well determined by dipole-dipole surveys (Pelton et al, 1978).

The inversion results for parameterization 3 are shown in Figure 5. The final positions of the α centers are shown by the solid circles. The one standard deviation error bars indicate that the depths to the top α centers and their positions along the profile are fairly well determined (±63 percent and ±.13 units, respectively) while the depth extent, as implied by the position of the lower α centers, is very poorly determined. Table 2 shows the parameter statistics and correlation coefficients. High correlations between α center coefficients C and background value B were virtually always obtained. The reason for this is easily explained by Figure 4, noting that the $1/R$ component of conductivity fall-off (i.e., $\sigma - B^2 + 2BC/R + C^2/R^2$) is controlled by the product of B and C. The correlation is reduced by data containing more samples distant from the inhomogeneity. The remainder of the large correlation coefficients are all in some way associated with the very poorly determined depth to the lower α centers.

These inversion results point out two serious defects in this modeling scheme. The first is that, although the location of the top α center is fairly well determined, we are given no clear cut indication of the actual depth to the top of the conductor. We may, however, be fairly confident that the α center position determined by inversion represents a maximum depth. The second defect is that we have no way of deducing the actual conductivity of the causative body from the α centers. This has been observed by practitioners of 2-D inversion using prismatic models who find that, without narrow constraints on prism boundaries, the conductivity distribution is very poorly determined from surface data (Oristaglio and Worthington, 1980).

Ten iterations for parameterization three required 18 sec on the University of Utah Univac 1108 and cost $.07. Figure 6 shows the convergence.

Test case 2: Dey and Morrison Basin and Range geothermal model

This model is shown in Figure 7. Data from line 1 and line 4 were inverted simultaneously. The initial guess is indicated in Figure 7 by the open circles. The small circles near the surface represent a distribution of α centers sufficient to account for the near-surface conductive layer and the more conductive material to the left of the vertical contact. The positions of these were kept constant, but their coefficients were included as inversion parameters. Four α centers were used to approximate the deeper conductive prism. Their intercenter geometry was specified but the position of the array was included as another inversion parameter.

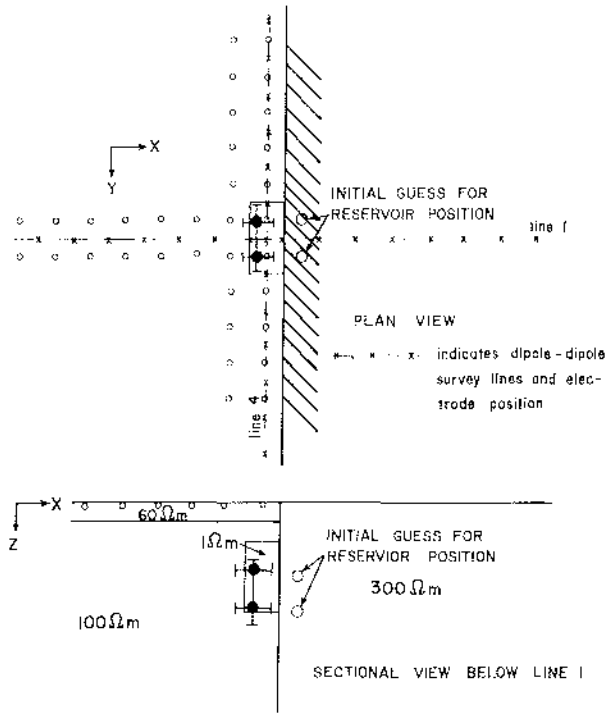

FIG. 7. Plan and profile view of Dey and Morrison Basin and Range geothermal model. Small open circles indicate position of surface α center distribution sufficient to account for more conductive material to left of contact. Large open circles show initial guess α center representation of reservoir. Solid circles indicate inverted position of reservoir with one standard deviation error bars on position.

This is tantamount to assuming that one knew approximately the size of the reservoir but not its location.

The theoretical data from lines 1 and 4 are shown in Figure 8. Initially the data from line 1 were inverted along with the off-profile position of the reservoir specified. All attempts to locate the reservoir failed; instead, the reaction was simply to remove the 3-D inhomogeneity. This is not particularly surprising when, as Dey and Morrison point out, the difference between data along line 1 with the prism and data along line 1 without the prism is slight. The inclusion of the line 4 profile greatly improved the situation. Since we were simultaneously inverting data from orthogonal traverses, there was no further need to specify the lateral position of the prism with respect to line 1. The simultaneous inversion placed all four prism α centers within the location of the hypothetical reservoir.

The resultant position of the centers and their one standard deviation error bars are shown in plan and profile in Figures 7 and 8 by the solid circles. Figure 8 shows the resultant best fit pseudosections. These represent a data fit of approximately 30 percent.

The parameter statistics (Table 3) indicate that this combination of parameters and data sets results in a well-determined model with no highly correlated parameters.

Five iterations for this group of parameters, simultaneously inverting to both data sets, took 5 minutes and cost $4.20.

Test case 3: Parallel dikes

This model is shown in Figure 9. The profile is perpendicular to, and bisects, the dikes, each of which is eight dipole lengths in strike extent.

The difficult aspect of inverting these data is that there is a rather attractive local chi-square minimum corresponding to a

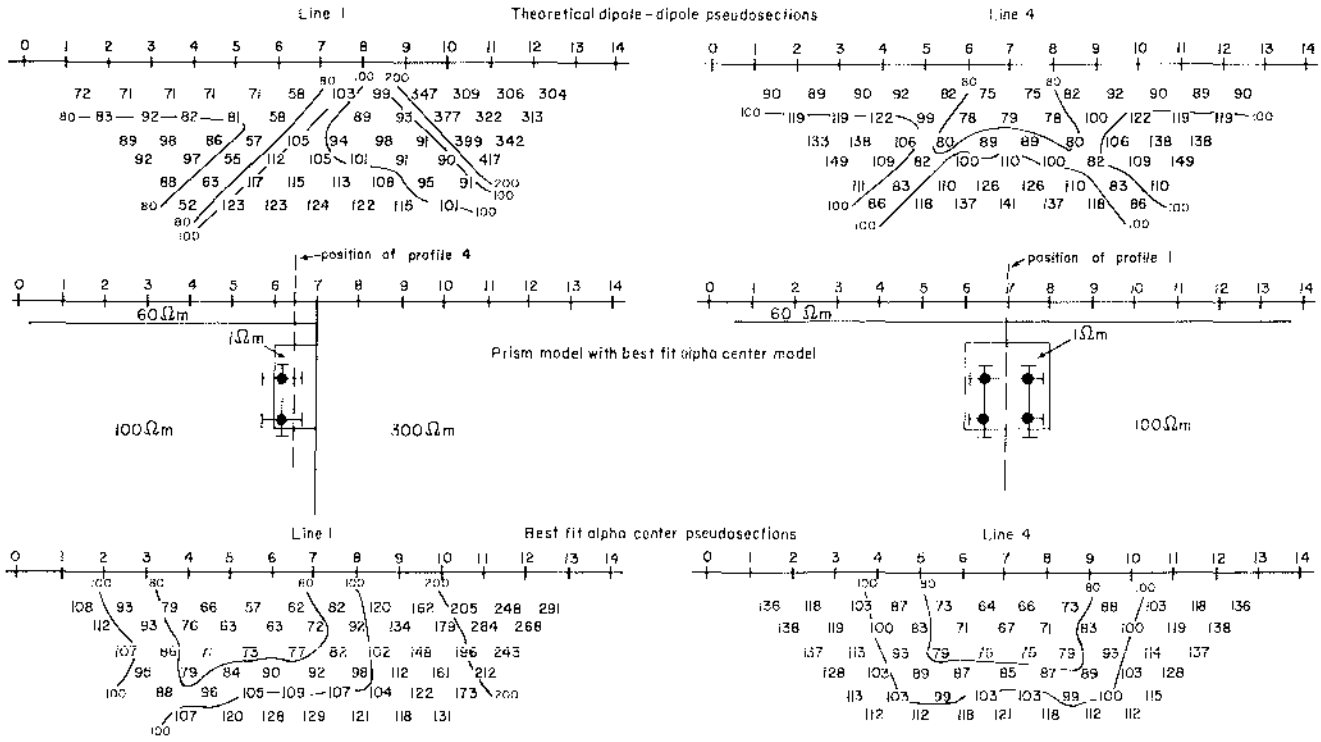

FIG. 8. Test case 2: results of simultaneous inversion of data from orthogonal profiles (line 1 and line 4) of Dey and Morrison Basin and Range geothermal model. The final positions of the four α centers used to mimic the reservoir are shown as the solid circles projected on the appropriate plane. The one standard deviation error bars are also shown. For convenience a dipole length of 100 m was chosen.

Table 3. Alpha center parameters, parameter statistics, and correlation coefficients for Dey and Morrison Basin and Range geothermal model.

Parameters	Inverted Model	Parameter Statistics	Correlation Coefficients					
B	$.024\sqrt{S/m}$	±28%	1.0					
$C_{Overburden}$	$.19\sqrt{Sm}$	±20%	-.69	1.0				
$C_{Reservoir}$	$1.25\sqrt{Sm}$	±24%	-.14	-.58	1.0			
$x_{Center\ Res.}$	617m	±48m	-.61	.69	-.30	1.0		
$y_{Center\ Res.}$	699m	±35m	.0	-.01	.01	.0	1.0	
$z_{Top.\ Res.}$	184m	±21%	-.44	.11	.55	.15	-.01	1.0

single large, deep conductor located at the center of the profile. The α center difference in data fit between the local and the "true" minima is only three percent. The situation is aggravated by the low-contrast ($\rho_2/\rho_1 = .2$) bodies involved, but the major difficulty is due to the inability of the α response to duplicate the high apparent resistivities between electrodes 7 and 9 at $n = 1$.

Three parameterizations were attempted. The first two involved starting with α centers locked together to form two separate vertical dikes with inversion variables being the background conductivity (B), coefficient for the left dike (C_{left}), coefficient for the right dike (C_{right}), position of the left dike along the profile (x_{left}), and the position of the right dike along the profile (x_{right}). The strike position of the dikes was held constant since we have only one profile. The difference between these two parameterizations was that one included as variables the depth (z_{left} and z_{right}) of each dike while for the other the depth was specified and held constant.

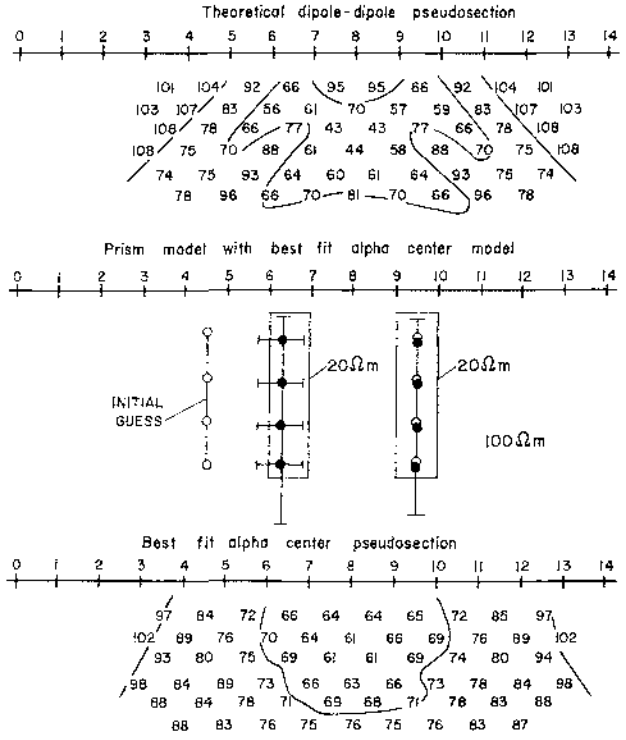

FIG. 9. Test case 3: two parallel dikes. Inversion results using α centers to fit data from prismatic model of two parallel, finite-length vertical dikes. The dikes are bisected by the profile. Solid circles show projection of final α center positions with associated one standard deviation error bars. A dipole length of 100 m was used for the calculations.

In the cases where the depth was a variable, the inversion process converged to the local minimum. Only when the depth was specified were the correct positions along the profile determined. This is certainly a serious constraint since in practice one would rarely have a better idea of the depth to the top of a body than of its position along the profile. Perhaps a better initial guess would remedy the problem, but it is probably safe to say that the false minimum is a broad one capable of engulfing all but the best of initial guesses.

The third parameterization represents a more practical application of inversion in which the position along the profile of one body is known. The addition of this information deprives the solution of the single central body local minimum, resulting in a very stable inverse. Included as inversion parameters were the background (B), the position along the profile (x_{left}) and depth (z_{left}) of the left dike, the coefficients of both dikes (C_{left} and C_{right}), and the depth of the right dike (z_{right}).

The initial guess α center positions are shown in Figure 9 as the open circles while the inverted α center positions are the solid circles. Figure 9 also shows the resultant best fit pseudo-section. This represents a data fit of approximately 19 percent. Parameter statistics are listed in Table 4.

Thirteen iterations required 5.5 minutes and cost $7.40.

FIELD EXAMPLES

To test the ability of α center inversion to locate conductive bodies in the presence of geologic noise, we chose data from three massive sulfide environments and a geothermal area. The only available data for each of these test cases are from a single profile; therefore, the off-profile geometry of the conductor was held fixed. In the massive sulfide test cases, the off-profile geometry was known from drillhole information.

Field example 1: Que River, N. W. Tasmania

The field data from line 7350N and simplified geologic cross-section are shown in Figure 10 (Webster and Skey, 1977). Figure 11 is a plan view of the massive sulfide ore outline.

Table 4. Alpha center parameters, parameter statistics, and correlation coefficients for test case 3, two parallel vertical dikes.

Parameters	Inverted Model	Parameter Statistics	Correlation Coefficients					
B	$.06\sqrt{S/m}$	±17%	1.0					
C_{Left}	$.34\sqrt{Sm}$	+35%	-.41	1.0				
x_{Left}	637m	+59m	.38	.37	1.0			
z_{Left}	120m	±109%	-.21	.78	.22	1.0		
C_{Right}	$.37\sqrt{Sm}$	±42%	-.72	-.28	-.67	-.21	1.0	
z_{Right}	125m	±85%	-.41	-.17	-.25	-.07	.73	1.0

An effective approach to invert real field data is initially to fix the depth to the top of the conductive zones and invert to background and conductor coefficients and positions along the profile. Once a minimum is obtained for this parameterization, the depth to the conductive zone is added as a new inversion variable. This approach was used on the Que River data allowing both P and S conductor parameters to vary independently. The result was a correct placement of the large, shallow S conductor beneath 5274E with the P conductor located at approximately 5250E. S and P conductor parameters were highly correlated, so we decided to fix the position of the S conductor and search only for the position (x_p, z_p) of the P conductor and coefficients C_s and C_p. This parameterization (regardless of any reasonable initial guess) resulted consistently in a conductor being placed deep below the electrode at 5250E. One might conclude that within the data fit error (approximately 120 percent), there is no dc resistivity information about a P conductor beneath 5150E.

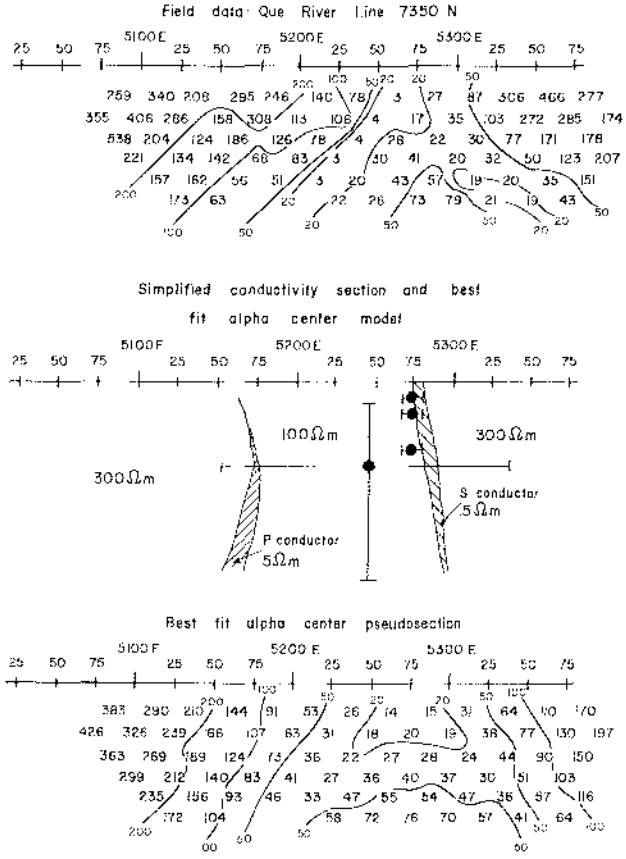

FIG. 10. Field example 1: Que River line 7350N. Inversion results showing field data, best fit pseudo-section, and α center model. Error bars represent one standard deviation. Note that although the S conductor has been precisely located, the inversion scheme failed to locate the deeper P conductor.

At this point we should define the components of "data fit error" with reference to real field data. The first component is measurement error which, for modern equipment in conductive terrains, is perhaps of order 5 percent. The second component is geologic noise—the response of small (or possibly large) scale inhomogeneities not directly associated with the sought after ore body. The third component is actually very difficult to separate from geologic noise, and that results in the possibility, or inevitability, of the wrong forward problem being done. Doing the wrong forward problem may be further subdivided into (1) the ability of a model conductivity distribution to fit what is actually in the subsurface, and (2) the adequacy of, or our interest in, modeling the geologic noise reflected in the field data.

We have found that using an α center model to fit theoretical data from conductive prisms usually results in a data fit error in the neighborhood of 20 to 30 percent.

To summarize, unless we really know the exact subsurface conductivity distribution, it is impossible to separate the geologic noise component of data fit error from the component due to doing the wrong forward problem.

The model statistics and correlation coefficients for the last parameterization are shown in Table 5. Ten iterations required 1.5 minutes and cost $1.90.

Field example 2: Woodlawn, New South Wales, Australia

Field data from this massive sulfide prospect are shown in Figure 12 (Tyne et al, 1978). As shown in the plan view (Figure 13), the profile crossed the northern edge of the near vertical ore body at an angle of approximately 30 degrees.

Initial parameterization took into account only variation in parameters B, and C, and position along the profile. From an initial guess shown by open circles in Figures 12 and 13, the position of the α described body was moved horizontally along the

Table 5. Alpha center parameters, parameter statistics, and correlation coefficients for field example 1, Que River, N.W. Tasmania.

Parameters	Inverted Model	Parameter Statistics	Correlation Coefficients			
C_s	$.313\sqrt{Sm}$	+58%	1.0			
C_p	$.23\sqrt{Sm}$	±250%	-.98	1.0		
x_p	5248m	±94m	-.91	+.91	1.0	
z_p	55m	+141%	.53	-.37	-.45	1.0
B	$5\times10^{-4}\sqrt{S/m}$	poorly determined parameter - fixed from earlier inversion				
x_s	5274m	±8m - fixed from earlier inversion				
z_s	fixed as shown in Figure 14					

profile to approximate the actual position of the conductive (approximately 1 Ω-m) massive sulfide body.

At this point we reparameterized to include also the depth of the α centers, using as an initial guess the results from the first inversion. This resulted in an insignificant position adjustment along the profile and a slight increase in the depth to the top α center from 15 to 18 m. The final positions of the centers with one standard deviation error bars are shown by the solid circles in Figures 12 and 13. These results would certainly be accurate enough to locate a drillhole correctly along the profile.

Table 6 shows the parameter statistics and correlation coefficients for the final parameterization. The data fit was approximately 160 percent. Each inversion took from 40 to 50 sec for 10 iterations.

Field example 3: Elura, New South Wales, Australia

The area in the vicinity of the Elura prospect is flat with extensive alluvial cover and little outcrop (Ogilvy, 1976). There is no surface expression of mineralization. The massive sulfide ore body is a near-vertical pipe (McCracken, personal communication) below approximately 90 m of overburden in a host of steeply dipping sediments.

The data and outline of the ore body are shown in Figure 14. The dipole length is 30.48 m. Due to the abundant geologic noise and depth of burial, the inversion scheme failed to locate the conductor. The approach was to attempt to fit the near-surface response with a surface α center distribution, then hold their positions

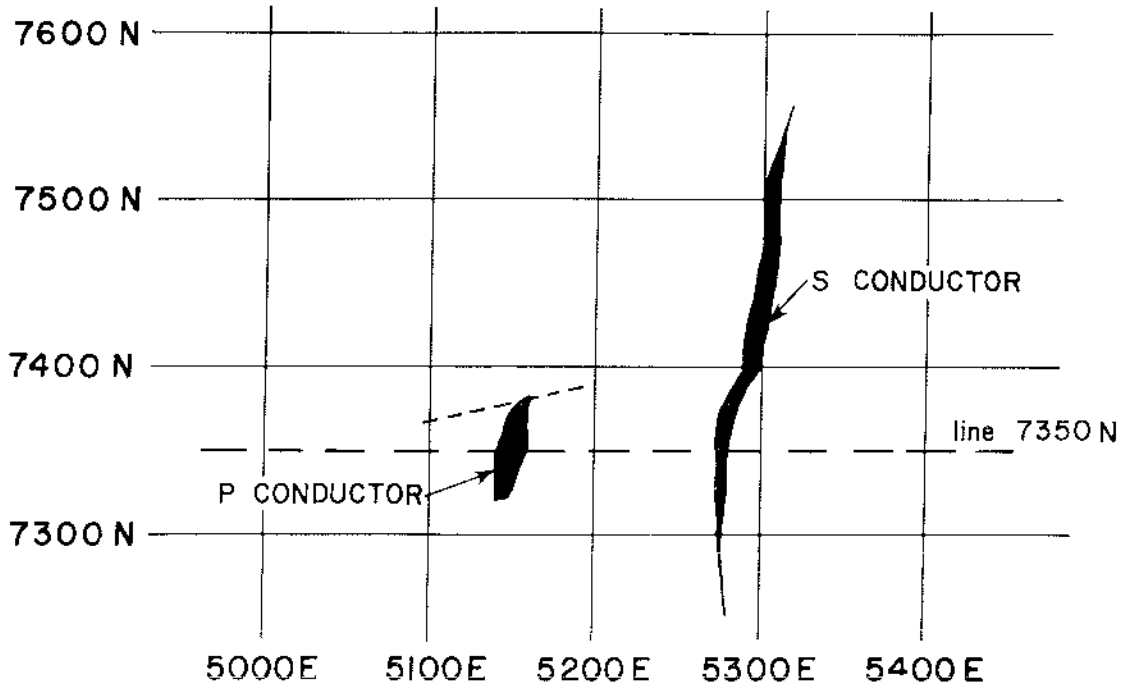

FIG. 11. Plan view showing locations of *P* and *S* conductors with respect to line 7350N, Que River, N.W. Tasmania.

Table 6. Alpha center parameters, parameter statistics, and correlation coefficients for field example 2, Woodlawn, N.S.W., Australia.

Parameters	Inverted Model	Parameter Statistics	Correlation Coefficients			
B	$.02\sqrt{S/m}$	±167%	1.0			
C	$.37\sqrt{Sm}$	±33%	-.89	1.0		
x	253m	±12m	.14	-.08	1.0	
z	18m	±162%	-.58	.81	-.05	1.0

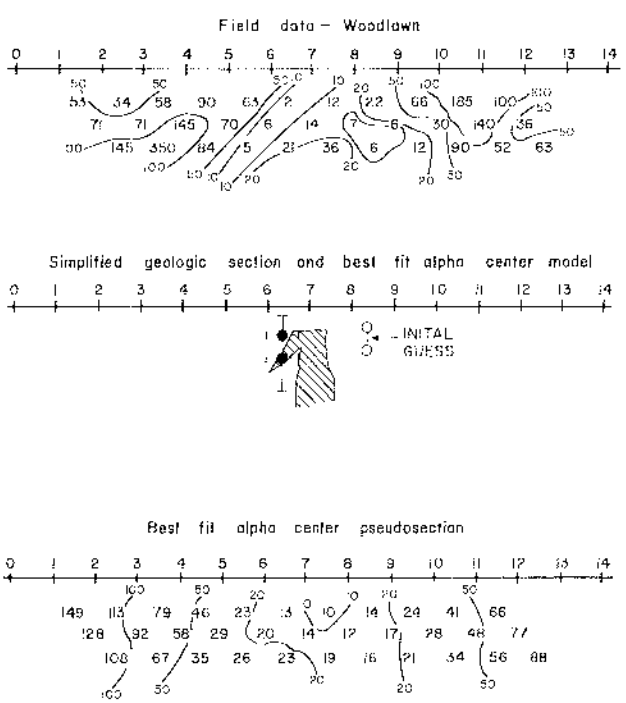

FIG. 12. Field example 2: Woodlawn, N.S.W., Australia. Inversion results showing field data, best-fit pseudo-section, and α center model. Initial guess α center positions are the open circles. Electrode six represents a local position along the profile of 243.8 m with a dipole length of 30.48 m.

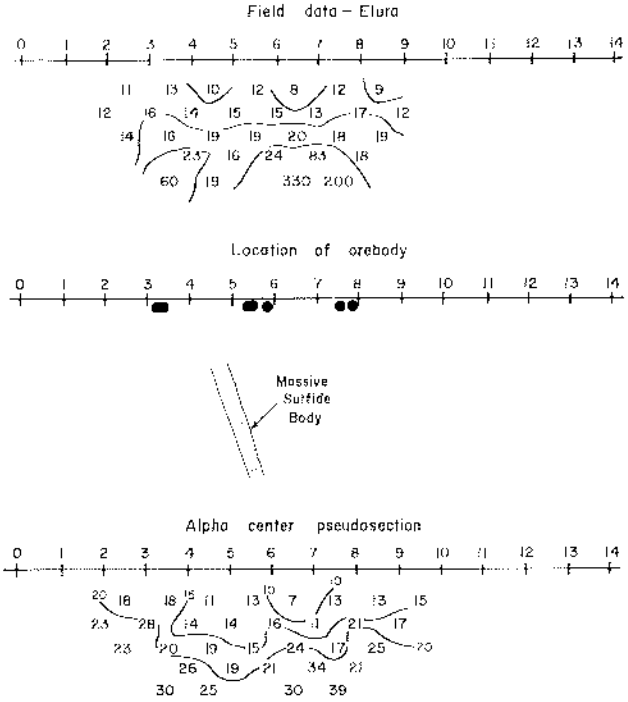

FIG. 14. Field example 3: Elura. Inversion results showing the inability of an α center model to determine the position of the deep vertical conductor in a conductive host. All α center parameters were undetermined. The dipole length is 100 m.

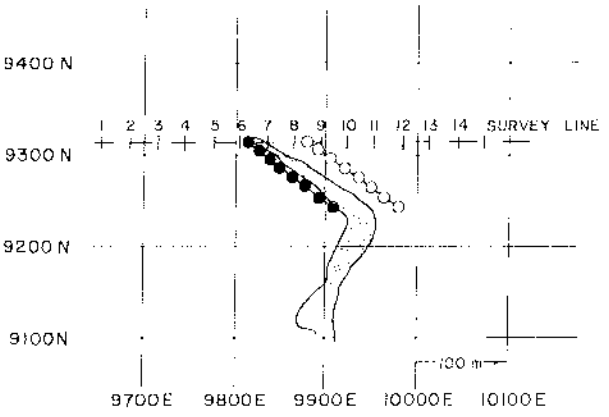

FIG. 13. Plan view showing position of massive sulfides at base of gossan with respect to survey line and electrode positions. Initial guess α center positions are open circles, while solid circles represent the inverted position of the α-defined conductive inhomogeneity, Woodlawn, N.S. W., Australia.

constant and invert to the position of an α center defined vertical cylinder. The inverted section in Figure 14 represents the α approximation to the near-surface noise. All attempts to locate the vertical conductor failed. The inversion routine simply removed the cylindrical conductor from the area of interest.

The data fit is approximately 75 percent.

Field example 4: Black Rock Desert, Utah

The data shown in Figure 15 are from the north portion of a 3 km multifrequency dipole-dipole survey extending north for 33 km from the north end of the Mineral Range. The pseudosection reflects the apparent resistivity data from the low-frequency asymptote. A deep drillhole 3 km west of the north end of the Mineral Range is the only local geologic control. The lithologic log reveals approximately 1 km of Pleistocene sediments overlying Paleozoic sediments. The basalt and rhyolite flows shown in Figure 16 have been dated at 2.1 to 2.2 mybp. The Cambrian sediments

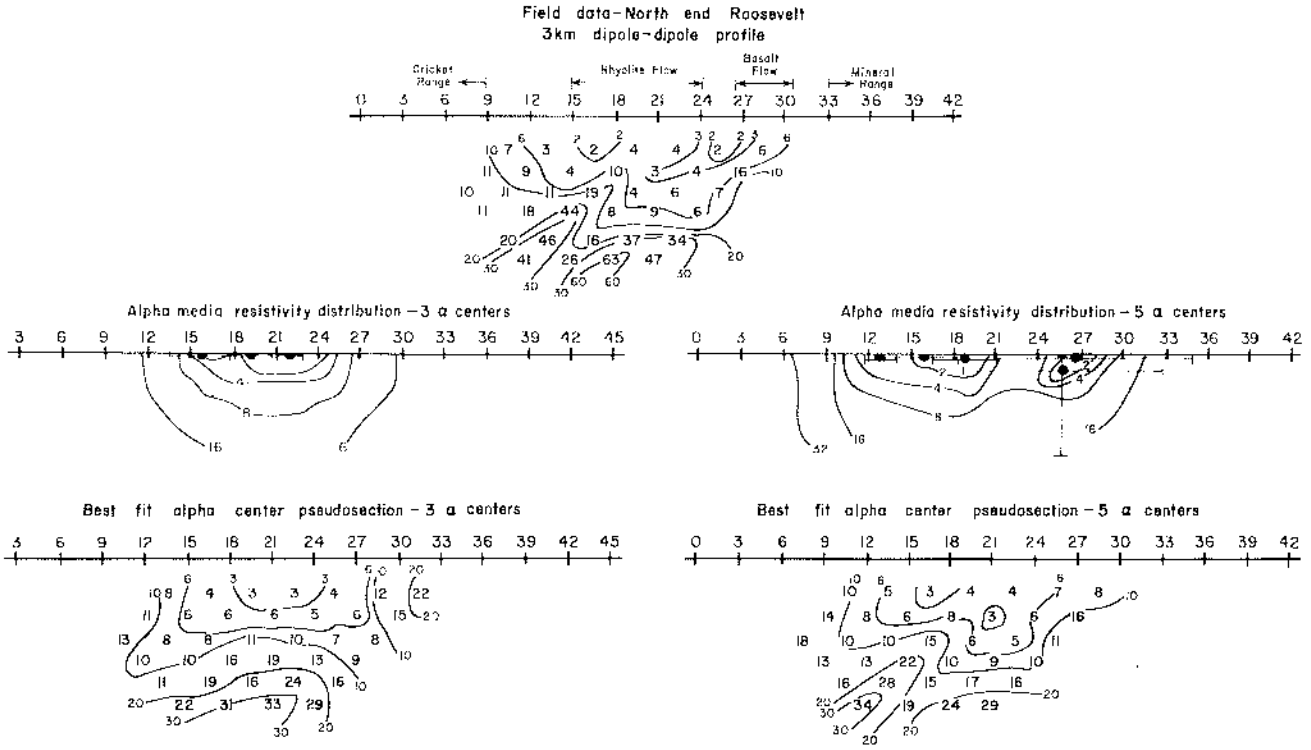

FIG. 15. Field example 4: Black Rock Desert, Utah. Two sets of inversion results illustrating the trade-off between data fit and parameter resolution when more α centers are used in the inverse solution. The plots to the left show the results when only three α centers are used to define the conductivity distribution, while those on the right show the results for five centers. If any deep conductors exist in this region, the α center inversion scheme failed to discriminate between their response and the near-surface conductive areas. The dipole length is 3 km.

comprising the Cricket Range just to the west of the profile are also present in thrusts at the north end of the Mineral Range. Water was virtually always encountered in shallow drillholes which penetrated the basalt and rhyolite flows.

Since only one profile was available, we used what meager geologic information we had in constraining the α centers. The inversion routine insisted on only shallow conductors, so the off-profile centers played a negligible role in the interpretation. At this point all α centers were constrained to lie immediately beneath the profile.

The two different inversion results illustrate the trade-off between data fit and parameter resolution. When three α centers are used, the data fit error is 97 percent and the α center parameters are fairly well determined (Table 7a). When five α centers are used, the data fit improves to 73 percent at the expense of parameter resolution (Table 7b).

The first model with three α centers defines, generally, the near-surface conductive zone due to the sedimentary fill between the Cricket Range and the Mineral Range. The two additional α centers improve the fit by defining a conductive zone between the rhyolite and basalt flows (stations 24–27). The location of the deepest α center is very poorly determined, indicating that from this single profile not much can be said about the conductive zone.

This example serves as an illustration of how the inversion

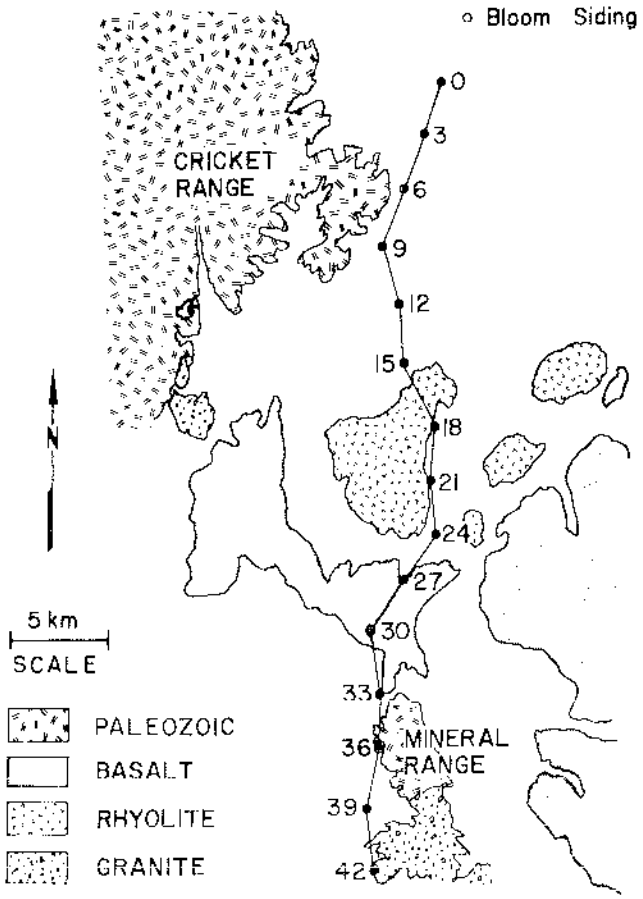

FIG. 16. Area map showing the north end of the Black Rock Desert 3-km dipole-dipole survey line near the Roosevelt Hot Springs KGRA, Utah.

Table 7. Alpha center parameters, parameter statistics on correlation coefficients for two different parameterizations of the Roosevelt Hot Springs KGRA. (a) Three α centers, (b) five α centers. Where depths are not shown, they were constrained to be 10 m.

Parameters	Inverted Model	Parameter Statistics	Correlation Coefficients										
a													
B	$.074\sqrt{S/m}$	±71%	1.0										
C_1	$321.\sqrt{Sm}$	±35%	-.34	1.0									
x_1	16.7km	±1.4km	-.11	-.13	1.0								
C_2	$296.\sqrt{Sm}$	±47%	-.47	-.33	.60	1.0							
x_2	24.4km	±.9km	.17	-.29	.05	.15	1.0						
C_3	$112.\sqrt{Sm}$	±87%	-.24	-.13	-.57	-.31	-.14	1.0					
x_3	13.2km	±2.2km	-.20	.07	-.05	.13	-.02	.03	1.0				
b													
B	$.024\sqrt{S/m}$	undet.	1.0										
C_1	$72.6\sqrt{Sm}$	undet.	-.34	1.0									
x_1	26.9km	±8.6km	-.46	-.96	1.0								
C_2	$241.\sqrt{Sm}$	±130%	-.64	.28	.34	1.0							
x_2	16.0km	-2.8km	.62	-.23	-.29	-.75	1.0						
C_3	$260.\sqrt{Sm}$	±120%	.57	-.29	-.34	-.94	.86	1.0					
x_3	18.7km	±2.3km	.64	-.28	-.34	-.95	.87	.96	1.0				
C_4	$212.\sqrt{Sm}$	undet.	.33	-1.0	-.96	-.28	.23	.29	.28	1.0			
x_4	25.8km	.7km	-.32	.98	.92	.27	-.21	-.28	-.26	-.98	1.0		
z_4	1.34km	undet.	-.49	.91	.97	.33	-.28	-.34	-.32	-.90	.89	1.0	
C_5	$90.2\sqrt{Sm}$	±160%	-.59	.16	.24	.44	-.86	-.61	-.62	-.17	.14	.23	1.0
x_5	12.7 km	±1.3km	.44	-.18	-.23	-.51	.65	.55	.57	.19	-.17	-.21	-.49	1.0

algorithm could provide information to guide further exploration or a reasonable initial guess for more sophisticated and probably much more costly multidimensional forward modeling or inversion schemes. The cost of obtaining these results was $.07 for ten iterations.

DISCUSSION AND CONCLUSIONS

Using this very fast and simple forward solution, the dc response of complex 3-D bodies may be easily calculated. Inverting data from prismatic bodies shows that their response can usually be approximated to within 20 to 30 percent. Multiple bodies and problems of mixed dimension present no special complications, although greatest efficiency is achieved for compact bodies. The most severe limitation inherent in this α center formulation is the inability to approximate resistive bodies. Another limitation is the difficulty in determining the actual conductivity of prismatic bodies.

The field examples illustrate the capability of the inversion algorithm to determine, in most cases, the positions of conductive bodies in the presence of abundant geologic noise. The program size, including both instruction and data storage, is currently less than 15,000 words and could easily be decreased to 10,000 words with judicious programming. These storage requirements bring the program within reach of small truck-mounted computer systems such as those currently being employed in data acquisition systems. This application would make in-field data interpretation possible.

A practical approach to inverting actual field data was first to use any available geologic information to determine the gross conductor geometry (e.g., podiform mass, vertical dike, manto, etc.) and lock together several α centers to approximate this shape. Again using as much geologic information as possible, fix the depth to the body at some plausible figure and invert to the position along the profiles. After obtaining a minimum for this parameterization, include the depth to the conductor as a variable and invert again using the initial inversion results as a starting model.

ACKNOWLEDGMENTS

We wish to thank Dr. Misac Nabighian and Cassandra Hudson, one of Dr. George Jiracek's students, for introducing us to α centers.

We would also like to thank Dr. Gerald Hohmann, Dr. Michael Oristaglio, Bill Sanfilipo, and Phil Wannamaker for model results and valuable suggestions.

We gratefully acknowledge the financial support provided under DOE contract number DE-AC07-79ET27002 and NSF grant number AER 76-11155 A.

REFERENCES

Dey, A., and Morrison, H. F., 1979, Resistivity modeling for arbitrary shaped three-dimensional structures: Geophysics, v. 44, p. 753–780.

Edwards, R. N., Lee, H., and Nabighian, M. N., 1978, On the theory of magnetometric resistivity (MMR) methods: Geophysics, v. 43, p. 1176–1203.

Grant, F. S., and West, G. F., 1965, Interpretation theory in applied geophysics: New York, McGraw-Hill Book Co., Inc.

Inman, J. R., 1975, Resistivity inversion with ridge regression: Geophysics, v. 40, p. 798–817.

Ogilvy, R. D., 1976, Geophysical survey, Elura prospect, Cobar, New South Wales, 1974: Australia Bur. of Min. Res. rep., Record 1976/47.

Oristaglio, M. L., and Worthington, M. H., 1980, Inversion of surface and borehole electromagnetic data for two-dimensional electrical conductivity models: Geophys. Prosp., p. 633–657.

Pelton, W. H., Rijo, L., and Swift, C. M., Jr., 1978, Inversion of two-dimensional resistivity and induced-polarization data: Geophysics, v. 43, p. 788–803.

Petrick, W. R., Pelton, W. H., and Ward, S. H., 1977, Ridge regression applied to crustal resistivity sounding data from South Africa: Geophysics, v. 42, p. 995–1005.

Rijo, L., 1977, Electromagnetic modeling by the finite element method: Ph.D. thesis, Univ. of Utah.

Rijo, L., Pelton, W. H., Feitosa, E. C., and Ward, S. H., 1977, Interpretation of apparent resistivity data from Apodi Valley, RGN, Brazil: Geophysics, v. 42, p. 811–822.

Stefanescu, S., 1970, Nouvelles applications de la théorie des milieux alpha harmoniques à la prospection électrique en courant continu: Geophys. Prosp., v. 18, p. 786–799.

Stefanescu, S., and Stefanescu, D., 1974, Mathematical models of conducting ore bodies for direct current electrical prospecting: Geophys. Prosp., v. 22, p. 246–260.

Stefanescu, S., and Radulescu, M., 1965, Modèles électrométriques de milieux α bidimensionnels: Rev. Roum. Geol., Géophys. et Geog. Série de Géophys., v. 9, p. 163–173.

Tyne, E. D., Agostini, A., Templeton, R. J., and Wootton, T. C., 1978, Electrical and potential field geophysical surveys over the Woodlawn deposit: Geol. Surv. New South Wales, Dep. of Mines, Geol. Sur. rep. no GS1978/005.

Webster, S. S., and Skey, E. H., 1977, Geophysical and geochemical case study of the Que River deposit, Tasmania, Australia: Proc. "Exploration 77," Ottawa.

APPENDIX
COMPARISON OF ALPHA CENTER RESPONSE WITH AN INFINITELY CONDUCTIVE SPHERE RESPONSE

Virtually all numerical and scale modeling schemes calculate responses due to bodies with piece-wise constant conductivity distributions. In an effort to bridge the gap between this type of conductivity structure and an α center conductivity distribution, we present the following simple analysis.

We start by writing the x-component electric field response E_{sx} of a sphere in a whole-space subject to a uniform x-directed electric field E_{0x} (Grant and West, 1965).

$$E_{sx}(x_p, y_p, z_p) = E_{0x}\left[1 - Ka^3\frac{1}{R^3}\left(1 - 3\frac{\Delta x^2}{R_2}\right)\right] \quad (A-1)$$

where

a = radius of the sphere,
K = reflection coefficient $(\sigma_2 - \sigma_1)/(\sigma_2 + 2\sigma_1)$,
σ_2 = conductivity of the sphere,
σ_1 = conductivity of the whole-space,

$$R = [\Delta x^2 + \Delta y^2 + \Delta z^2]^{1/2},\ R \geq a,$$
$$\Delta x = (x_p - x_c),$$
$$\Delta y = (y_p - y_c),$$
$$\Delta z = (z_p - z_c),$$

and the subscripts p and c refer to the positions of the field point and the center of the sphere, respectively.

The same field component $E_{\alpha x}$ due to a single α center in a whole-space is

$$E_{\alpha x}(x_p, y_p, z_p) = E_{0x}\left\{B + \frac{C}{R}\left[1 + \frac{\Delta x^2}{R^2}\right]\right\} B \Big/ \left[B + \frac{C}{R}\right]^2 \quad (A-2)$$

where

$$R = [\Delta x^2 + \Delta y^2 + \Delta z^2]^{1/2},$$
$$\Delta x = (x_p - x_\alpha),$$
$$\Delta y = (y_p - y_\alpha),$$
$$\Delta z = (z_p - z_\alpha),$$

B and C are the usual α center parameters, while the subscripts p and α refer to the position of the field point and the α center, respectively.

Figure A-1 shows a plot of equations (A–1) and (A–2) where $K = 1$ (infinitely conductive sphere) in equation (A–1). Results for two different sphere sizes and Δz values are shown. As is

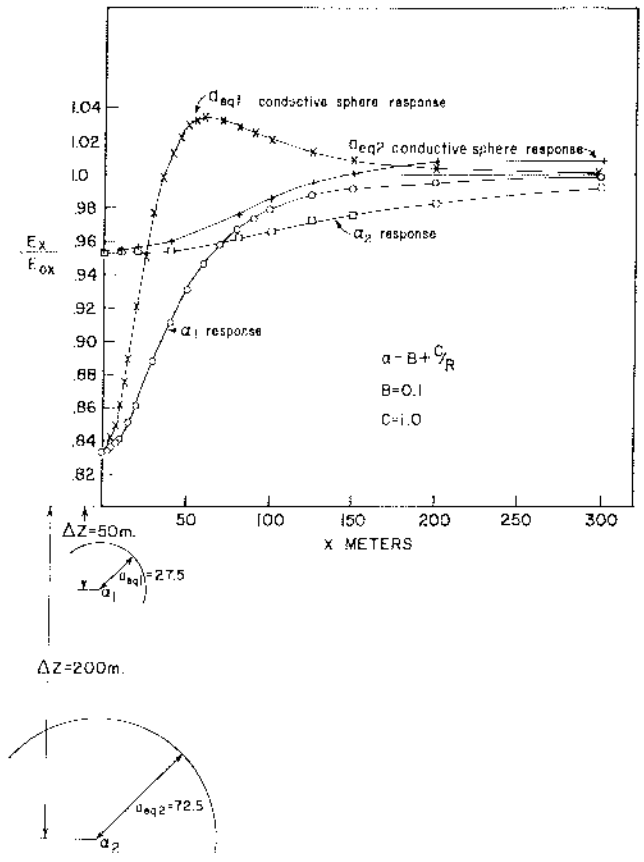

FIG. A–1. Comparison between α center and infinitely conductive sphere responses to a uniform x-directed electric field in a whole space. The results are for two different Δz values. (1) α_1 and $\alpha_{eq(1)}$ at $\Delta z = 50$ m, (2) α_2 and $\alpha_{eq(2)}$ at $\Delta Z = 200$ m. α_{eq} is obtained by substituting $B = .1$, $C = 1.0$, and Δz equation (18).

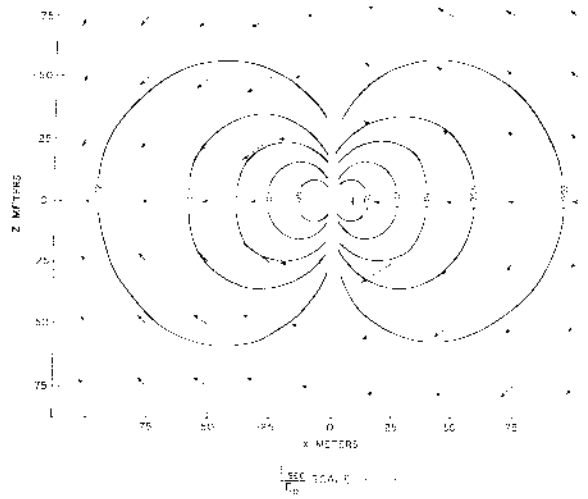

FIG. A–2. Plot of charge density and resultant secondary electric field pattern for one α center in a whole space subject to a uniform x-directed electric field E_{0x}. Plot is in plane $(x, 0, z)$ through an α center located at origin. Contours indicate values of $\rho/\varepsilon_0 E_0$ and vectors are in terms of E_{sec}/E_0.

obvious from the plots, the α center response is not dipolar. An α center response can never exhibit the characteristic "overshoot" of dipolar responses.

We will now attempt to explain the reasons for this by calculating the charge density associated with an α center in a uniform electric field

$$\rho = \varepsilon_0 \nabla\sigma \cdot \nabla\phi/\sigma - \frac{2\varepsilon_0}{\alpha^2} \nabla\alpha \cdot (\nabla\psi - \psi\nabla\alpha/\alpha). \quad \text{(A–3)}$$

In terms of α center parameters the charge density at point p is

$$\rho(p) = 2E_{0x}\varepsilon_0 BC \frac{BR + 2C}{(BR + C)^3} \frac{\Delta x}{R}, \quad \text{(A–4)}$$

where the variables in equation (A–4) are the same as those defined for equation (A–2). Figure A–2 shows a plot of the charge density and the secondary electric field pattern on the plane $\Delta y = 0$. The response from this diffuse cloud of charge may be understood by integrating equation (A–4) over the volume defined by $\Delta x > 0$. The total charge in the right half-space is given by

$$Q = 2E_{0x}CB\pi\varepsilon_0 \int_0^\infty R^2 \frac{[BR + 2C]}{[BR + C]^3}\, dR. \quad \text{(A–5)}$$

If we pick an arbitrary hemispherical surface at point R_c, we can calculate the total charge in the regions $R < R_c$ and $R > R_c$. From equation (A–5) we have

$$Q = 2E_{0x}CB\pi\varepsilon_0 \left[\int_0^{R_c} \frac{BR^3}{[BR + C]^3}\, dR + \int_{R_c}^\infty \frac{BR^3}{[BR + C]^3}\, dR + \int_0^{R_c} \frac{2CR^2}{[BR + C]^3}\, dR + \int_{R_c}^\infty \frac{2CR^2}{[BR + C]^3}\, dR \right]. \quad \text{(A–6)}$$

All but the second of the integrals in equation (A–6) converge. For large R the integrand approaches a constant, indicating that no matter how far away from the α center you take R_c, the component of total charge due to the charge density remaining in the region beyond R_c is infinite. This forces the secondary electric field never to change sign and so it can never exactly duplicate a true dipolar field. Note that the total charge in the whole-space is zero since the component of total charge in $\Delta x < 0$ is opposite in sign from that in $\Delta x > 0$. Also, equation (A–6) is not divergent for any region; it simply states that a charge density will be supported at any point in α media where one is willing to expend the energy necessary to maintain a uniform electric field E_0.

Thus far, we have shown that an α center response is not dipolar and, furthermore, why it is not dipolar. We can still obtain some useful information concerning the parameters of a conductive sphere by considering the response directly above the sphere and α center, i.e., $\Delta x = 0$ and $\Delta y = 0$ in equations (A–1) and (A–2). Making these substitutions, then equating (A–1) and (A–2) and solving for Ka^3, we obtain

$$Ka^3 = \Delta z^3 \left(\frac{C}{B\Delta z + C} \right).$$

Therefore, in the simple case of a single α center, the inversion routine will supply all parameters on the right side of the equation, and from them an estimate of the reflection coefficient × volume product may be obtained.